THE ASTROPHYSICAL JOURNAL, 420:58–67, 1994 January 1

NEAR-INFRARED IMAGING OF LOW-REDSHIFT QUASAR HOST GALAXIES

K. K. McLEOD AND G. H. RIEKE
Steward Observatory, University of Arizona, Tucson, AZ 85721
Received 1993 May 13; accepted 1993 July 8

ABSTRACT

We present H-band images of a complete sample of 24 low-luminosity quasars selected from the Bright Quasar Survey. We detect the quasar host galaxy in at least 22 of these objects. We use a one-dimensional radial profile analysis to remove the contribution of the nucleus to the H-band light and to investigate the properties of the underlying galaxy. In most cases, the galaxy profiles are fitted better by exponential disk models than by de Vaucouleurs models. The average galaxy magnitude is $\langle M_H \rangle = -23.9$ mag, which is approximately the H magnitude of an L^* galaxy. This result argues against the quasar activity being triggered by the merger of two large galaxies. No quasar host galaxies have inclinations greater than 60°, suggesting that obscuration near the active nucleus hides many of these objects from our view; their space density could be underestimated by a factor of ~ 2. We combine our results with previously published results from CCD imaging to show that the galaxies we detect are about 0.5 mag bluer in $V-H$ than normal galaxies. Such colors can arise from a heightened level of star formation compared with normal galaxies and are consistent with these galaxies having been the sites of luminous starbursts about 10^8 yr ago.

Subject headings: galaxies: photometry — infrared: galaxies — quasars: general

1. INTRODUCTION

More than a decade ago, optical imagery and spectroscopy showed that low-redshift quasars live in the nuclei of galaxies. Detailed studies of the host galaxies are needed if we are to understand the active galactic nucleus (AGN) phenomenon and galaxy evolution. Host galaxy studies can help us to understand how QSOs differ from other classes of AGN, what kinds of galaxies are able to "feed" an active nucleus, and whether all galaxies go through an active phase at some point in their lives. They can show us what effects the active nucleus has on star formation in the galaxy, and what kinds of effects might result in correlations between global galaxy properties and nuclear activity. They can also help us test the currently popular hypothesis that QSOs form following the merger of two gas-rich spiral galaxies.

The first attempts to image QSO hosts used photographic plates. These early studies met with limited success because of the nonlinearity inherent in photography; disentangling the galaxian light from the overwhelmingly bright nuclear light requires a highly linear detector. Nonetheless, many galaxies were imaged and several interesting properties were discovered. For example, a photographic survey of 78 quasars (Hutchings, Crampton, & Campbell 1984; Hutchings et al. 1984) indicated that (i) there are differences between galaxies of radio and optically selected QSOs; (ii) there may be a correlation between nuclear and galaxian luminosity, in the sense that more luminous quasars reside in more luminous galaxies; and (iii) many of the QSOs appear to be interacting with other galaxies.

More recently, the use of CCD and other electronic detectors has obviated many of the difficulties of photographic imaging. The conclusions based on CCD studies of QSO hosts have been varied and sometimes conflicting (see Véron-Cetty & Woltjer 1990, hereafter VW, for a summary). Many of the results are suspect because of observational selection effects and effects of sample selection. As pointed out by VW, comparing properties of radio-loud and radio-quiet quasars requires caution because the radio-loud quasars are generally more luminous and, hence, at higher redshifts in magnitude-limited samples. Also, the apparent correlation between nuclear and galaxian luminosity might result from observational selection effects. Low-luminosity quasars in high-luminosity galaxies might be excluded from quasar studies because these objects would be classified as Seyferts. Low-luminosity galaxies around high-luminosity quasars might escape detection because the quasar light overwhelms that of the galaxy and because these quasars are often at large redshifts (VW; Malkan 1984; Gehren et al. 1984).

Several recent CCD surveys have avoided some of these problems by careful sample selection. VW studied a complete sample of 36 nearby ($z < 0.5$), high-luminosity ($-24.6 > M_V > -26.6$ mag; $H_0 = 50$ km s^{-1} Mpc^{-1}) quasars from the VV catalog (Véron-Cetty & Véron 1984). Their sample is divided roughly equally between radio-loud and radio-quiet QSOs. Hutchings (1987), Hutchings, Johnson, & Pyke (1988), and Hutchings, Janson, & Neff (1989) imaged a sample of 75 objects in the redshift range $0.1 < z < 0.5$. Their sample included roughly equal numbers of radio-loud QSOs, radio galaxies, and radio-quiet QSOs, well matched in V magnitude and redshift. Though their results differ somewhat in detail, these two groups agree on some general conclusions: (i) Radio galaxies and radio-loud quasar hosts galaxies have many similarities; both types may be ellipticals, albeit luminous and blue ones. (ii) Host galaxies of radio-quiet quasars are dimmer and many are consistent with being disk galaxies. (iii) Radial luminosity profiles are often ambiguous, with neither a disk model nor $r^{1/4}$ model preferred.

While these surveys made much improvement over other CCD studies, observations of QSO host galaxies at near-IR wavelengths offer hope for still more improvement. First, the spectral energy distributions (SEDs) of the host galaxies are likely to peak just longward of 1 μm, whereas the nuclear SEDs generally have local minima at about 1 μm (Sanders et al. 1989). Taking advantage of this happy coincidence by observing in the H band, we can observe the galaxiean light with less contamination from the nucleus than is possible at optical

wavelengths; thus, removal of the nuclear point source should be easier. Second, since IR images will show the galaxy's red stellar population, they will show the mass-tracing component of the galaxy. By contrast, CCD studies might ascribe high mass to a galaxy whose visible light output has been boosted by recent star formation. A related argument is that infrared images should yield the underlying galaxy structure with little influence from regions of recent star formation. Third, IR images do not suffer significant contamination from emission lines, which spectroscopy has shown to be substantial in the optical (e.g., Boroson, Persson, & Oke 1985). We note that the VW survey partly circumvented this problem by observing in the *i* band, where strong optical emission lines such as [O III] 5007 Å do not contribute for low-redshift objects. Fourth, the IR data can be used along with optical data to determine host galaxy colors, an important step in investigating the effects of an active nucleus on the star formation properties of the galaxy.

Because of the development of highly linear, large-format IR arrays, it is now feasible to study active galaxies using near-IR imaging. Kotilainen et al. (1992) and Zitelli et al. (1993) have used IR arrays to observe some X-ray and optically selected Seyfert 1 galaxies, while Dunlop et al. (1993) have obtained *K*-band images of some radio-loud and radio-quiet quasars. The Dunlop et al. sample was carefully chosen to avoid some of the selection effects mentioned above. Their radio-quiet sample is well matched to the sample we describe here, though there are only three objects common to both studies.

In this paper, we report the first results of a program to study QSO host galaxies with H-band imaging. We have selected low-luminosity QSOs from a complete optically selected sample, the Bright Quasar Survey (Schmidt & Green 1983). We have chosen all of the QSOs between $-24.1 \leq M_B \leq -23$ (as reported in that paper; $H_0 = 50$ km s^{-1} Mpc^{-1} and $q_0 = 0.1$). The faint cutoff was chosen to exclude objects more commonly labeled as Seyferts; objects dimmer than this might have been excluded from the Bright Quasar Survey because they were seen to be extended. This sample has a total of 24 QSOs with mean redshift $\langle z \rangle \approx 0.1$ and maximum redshift $z = 0.161$. Because these QSOs are nearby (other studies of low-luminosity QSOs frequently have $\langle z \rangle = 0.3$), we can achieve high spatial resolution to assist in separating the extended light from the nuclear light.

2. OBSERVATIONS

We obtained IR images of the 24 quasars in our sample at the Steward Observatory 2.3 m telescope on Kitt Peak during the period 1992 May to 1993 April. The quasars in our sample, along with redshifts and observation dates, are listed in Table 1. The images were taken with a 256 × 256 IR array camera which used one of two NICMOS HgCdTe detector arrays. The second array, installed in the camera prior to our 1992 September observing run, provided increased quantum efficiency and greatly reduced the number of bad pixels compared with the first. We used an *H*-band filter to maximize the galaxian-to-nuclear light contrast and to observe the galaxies where the red stellar light is brightest. We chose the camera's coarse pixel scale, 0.″6 pixel^{-1}, because it gave adequate spatial resolution while providing a large enough field of view for us to find stars in the same field as the QSOs. The stars in each quasar field were used to determine the point spread function (PSF) for each image. One object, PG 1612+261, was observed with a slightly different instrument setup, using the camera's fine (0.″23 pixel^{-1}) scale. Typically, the seeing was about 1″.

TABLE 1

THE SAMPLE

PG #	z[a]	Date	P_{5GHz}[b] (10^{22} W Hz^{-1})
0050+124	0.061	1992 Sep 09	4.2
0804+761	0.100	1992 May 11	10
0838+770	0.131	1992 May 12	≤ 1.1
0844+349	0.064	1992 May 12	0.55
1001+054	0.161	1992 May 13	8.9
1114+445	0.144	1992 May 12	1.9
1115+407	0.154	1992 May 14	3.0
1211+143	0.085	1992 May 13	3.8[c]
1229+204	0.064	1993 Apr 07	1.2
1351+640	0.087	1992 May 11	44
1404+226	0.098	1992 May 12	4.2
1411+442	0.089	1992 May 12	2.1
1415+451	0.114	1992 May 14	2.2
1416−129	0.129	1992 May 13	26
1426+015	0.086	1992 May 13	3.8
1435−067	0.129	1992 May 13	1.3
1440+356	0.077	1992 May 14	4.3
1519+226	0.137	1992 May 11	12
1552+085	0.119	1992 May 14	4.9
1612+261	0.131	1992 May 12	37
1617+175	0.114	1992 May 11	11
1626+554	0.133	1992 May 14	1.3
2130+099	0.061	1992 Sep 09	3.3
2214+139	0.067	1992 Sep 09	0.47

[a] Schmidt & Green 1983.
[b] Kellerman et al. 1989.
[c] Derived from Miller, Rawlings, & Saunders 1993.

The data were obtained by taking a series of exposures with the QSO position varied in a raster pattern across the array. Each frame was offset from the previous frame by about 30″. The exposure time for each frame was about 40 s, which gave background-limited imagery without saturating the array on the bright quasar. Depending on placement of the PSF stars in the field, there were either nine or 16 frames in each raster pattern. Typically, three rasters were completed for each quasar. Several times throughout each night, IR photometric standard stars from the catalog by Elias et al. (1982) were observed in a similar manner. All of the quasars in our sample were observed during photometric conditions.

3. DATA REDUCTION

3.1. *Image Reduction*

To obtain a final image for an object, each set of raster frames was reduced separately and the results were combined afterward. The nine or 16 frames in each raster set were used along with a dark frame of the same exposure time to create median sky frames and normalized flat frames. These in turn were used to sky-subtract and flat-field the individual frames in the raster. The images were shifted to align them on the brightest quasar pixel, and combined by averaging to produce a final image for the raster. Bad pixels were excluded from the average through the use of a mask, and the minimum- and maximum-valued pixels at each position were thrown away before the final average was computed. For the four objects observed with the new array, no masking was necessary. Those images were aligned on the centroids of all objects of sufficient signal-to-noise (S/N) rather than on the brightest quasar pixel. Typically, three to four objects were used. Rejection of minimum- and maximum-valued pixels was still used.

A variety of tests confirmed that the procedures used to align the frames would not bias our results. We tried aligning on the brightest quasar pixels, on the quasar images' centroids, on the brightest pixels in stellar images, and on the centroids of a number of objects in the frames. All the results were similar. If anything, the procedure we adopted tended to "tighten up" the quasar image slightly compared with the alternatives, a result which might cause us to overestimate slightly the galaxy contribution to the total image.

To combine the raster sets for each object, we used a weighted average. We determined the weight of each frame by fitting a Gaussian curve to the inner part of the quasar radial profile. The weight was taken to be the square of the peak intensity of the Gaussian curve. In this way, we gave higher weight to frames with smaller widths (the peak intensity times the width was approximately constant). The resulting images have a central region (where the quasar is located) to which all of the original frames contribute, and outlying regions where only some of the original frames contribute because of the image offsets. Contour plots showing the central region of each reduced frame are shown in Figure 1 with contour levels given in Table 2. The object is obviously extended in most cases.

3.2. *Profile Extraction*

We used a one-dimensional technique to remove the contribution of the nucleus from each reduced quasar image. The one-dimensional radial profile for each object was obtained by using the ellipse fitting task in IRAF to compute the average pixel value in an elliptical annulus at each radius. The ellipse fits were carried out down to a surface brightness level at which S/N $\approx$ 1, where S/N is the mean value of intensity around an isophote divided by the rms deviation of intensities along the isophote. For most of the frames, this corresponded to $H \approx 21.3$ mag arcsec^{-2}.

We used the same technique to extract the radial profiles of stars from each image to determine the PSF. In each case, we selected a star that (i) was near the quasar, (ii) had good S/N, and (iii) was not saturated on the original frames. Here, "near the quasar" means the star was located in the central overlap region of all frames. In about half of the images, there was no suitable star in the central region. In these cases, we averaged normalized profiles of two or three stars from outlying parts of the image. Tests of this procedure on images which had both outlying stars and central stars gave excellent agreement. The radial profiles of our quasars and PSF stars are shown in Figure 2.

TABLE 2

CONTOUR PLOT LEGEND

	Contour (H mag arcsec^{-2})	
PG #	Low	High
0050+124	21.0	12.8
0804+761	21.0	14.1
0838+770	21.0	15.3
0844+349	21.0	14.1
1001+054	21.0	15.1
1114+445	21.0	14.3
1115+407	20.5	15.0
1211+143	20.5	13.7
1229+204	21.0	14.9
1351+640	21.0	14.9
1404+226	21.0	14.9
1411+442	20.5	13.4
1415+451	21.0	14.7
1416−129	21.0	15.3
1426+015	20.5	14.0
1435−067	21.0	14.8
1440+356	21.0	13.4
1519+226	21.5	14.8
1552+085	21.0	15.1
1612+261	21.0	14.8
1617+175	21.0	14.5
1626+554	21.0	15.8
2130+099	21.0	13.5
2214+139	20.0	14.3

3.3. *Profile Fitting*

To determine the properties of each galaxy, we first had to remove the contribution of the nucleus. We assumed that the nucleus was a point source with radial profile represented by the PSF profile. The PSF was normalized to have the same flux as the quasar at the innermost point of the profile, a radius of 1 pixel. We then subtracted progressively larger fractions of the PSF profile from the quasar profile. We stopped subtracting just before the resulting profile became nonmonotonic with radius, i.e., before the profile turned over at small radii. The resulting profile was then fitted with an exponential disk model with free parameters r_0 and s_0, the disk scale length and the central surface brightness, respectively. Finally, the total amount of light in the galaxy was computed from these parameters as $I_{\rm tot} = 2\pi r_0^2 s_0$. The results of these fits are listed in Table 3.

To check our results, we also experimented with subtracting the fraction of the PSF that minimized the rms residuals for an exponential disk model of the galaxy. The enclosed flux was the same to within about 15% $\pm$ 10%. In addition, the disk scale lengths and central surface brightnesses matched the original values very well. As another check, we also fitted an exponential disk law to only the outer parts of each unsubtracted quasar profile, outside the radius where the nucleus contributes. While the central surface brightnesses and disk scale lengths were sometimes different than for the subtracted fits, the enclosed fluxes were the same to within about 20%.

The disk fits we used did not include an $r^{1/4}$ contribution from a central bulge because there are not enough pixels across the inner parts of the galaxies to justify fitting an extra component. As a result, the disk scale lengths and central surface brightnesses derived are possibly in error. Any contribution of the bulge to the light of the PSF–subtracted profile will tend to decrease artificially the disk scale length while boosting the central surface brightness. As we show below, the disk scale lengths are typical of spiral galaxies, whereas the central surface brightnesses are slightly brighter than normal. We estimated the possible error due to neglect of the bulge component based on the study of Kent (1985). For the early-type spirals in his sample, the bulge contributes about 40% of the total r-band light, albeit with large scatter. For later types, the contribution is much less. We assume the bulge-to-disk ratio at H will be similar. While the disk models may not have the correct functional form to use at all radii, they account for at least some of the bulge light. Thus, we estimate that the total galaxy H fluxes are likely accurate to about 25%.

We experimented with fitting a de Vaucouleurs $r^{1/4}$ model for each galaxy, subtracting a fraction of the PSF that gave the

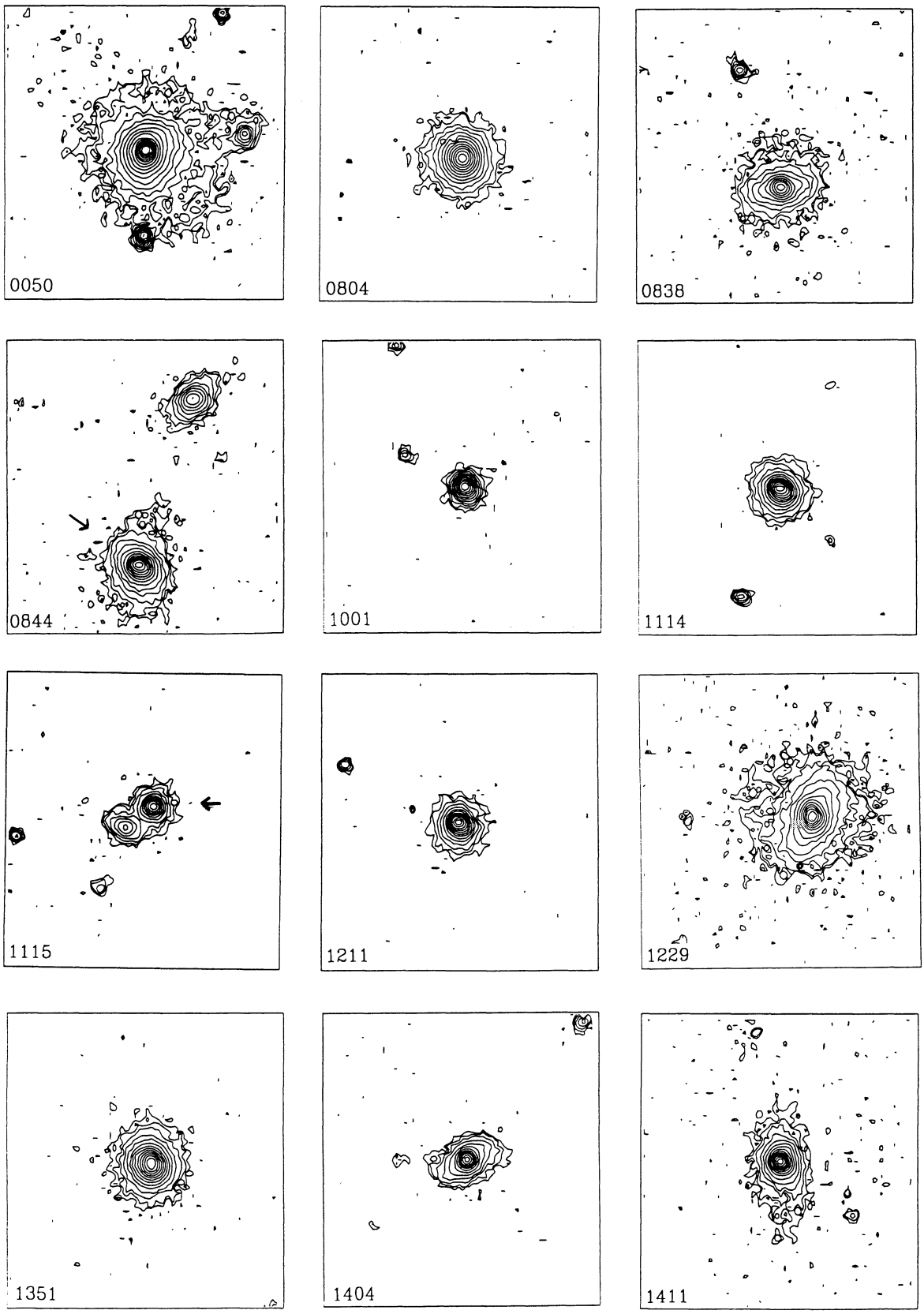

FIG. 1.—Contour plots showing the central 38 × 38″ region of each quasar image. Contours are in steps of 0.5 *H* mag arcsec^{-2}. The lowest contour level and peak surface brightness for each object are given in Table 2. North is down and east is to the left.

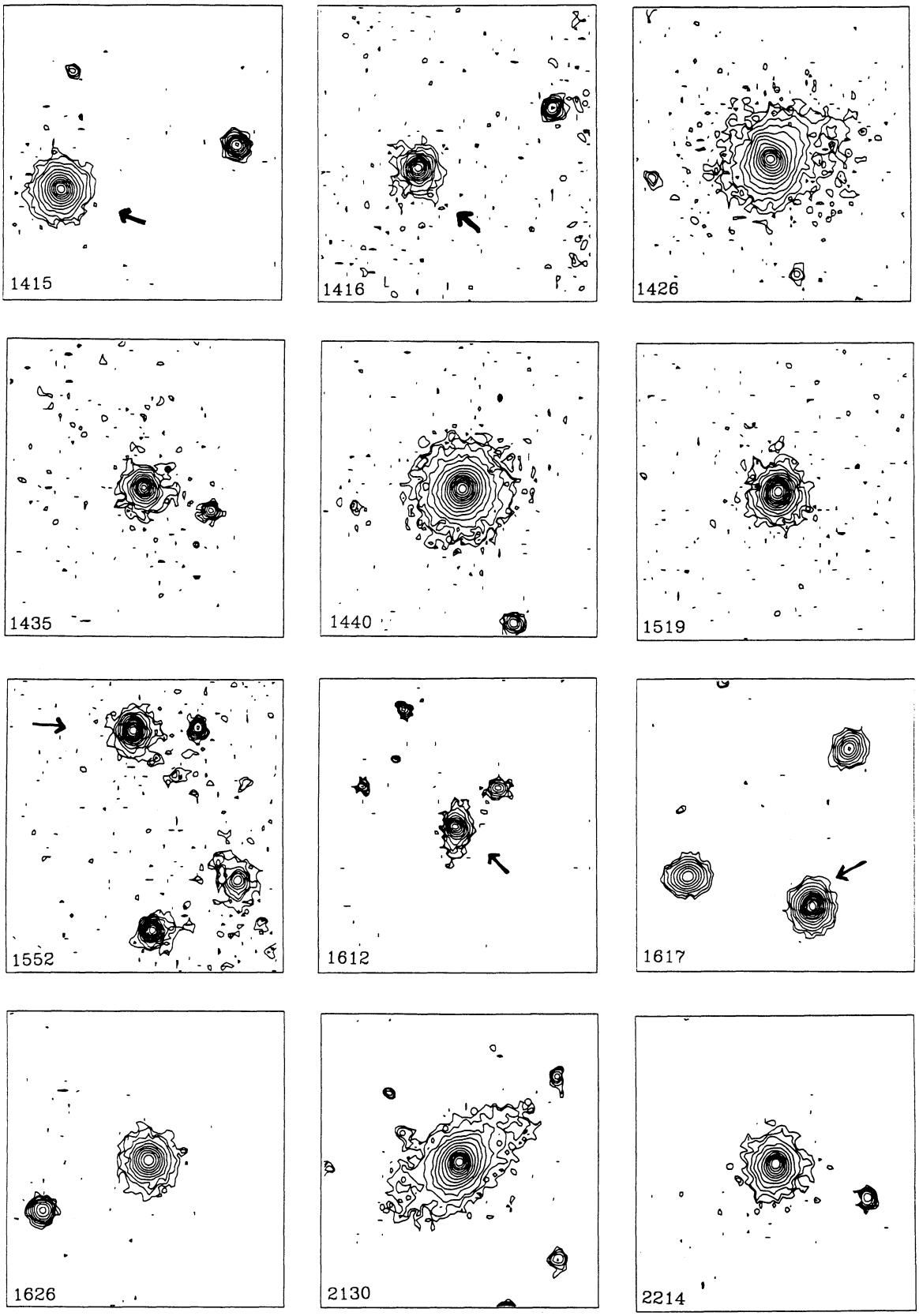

FIG. 1—*Continued*

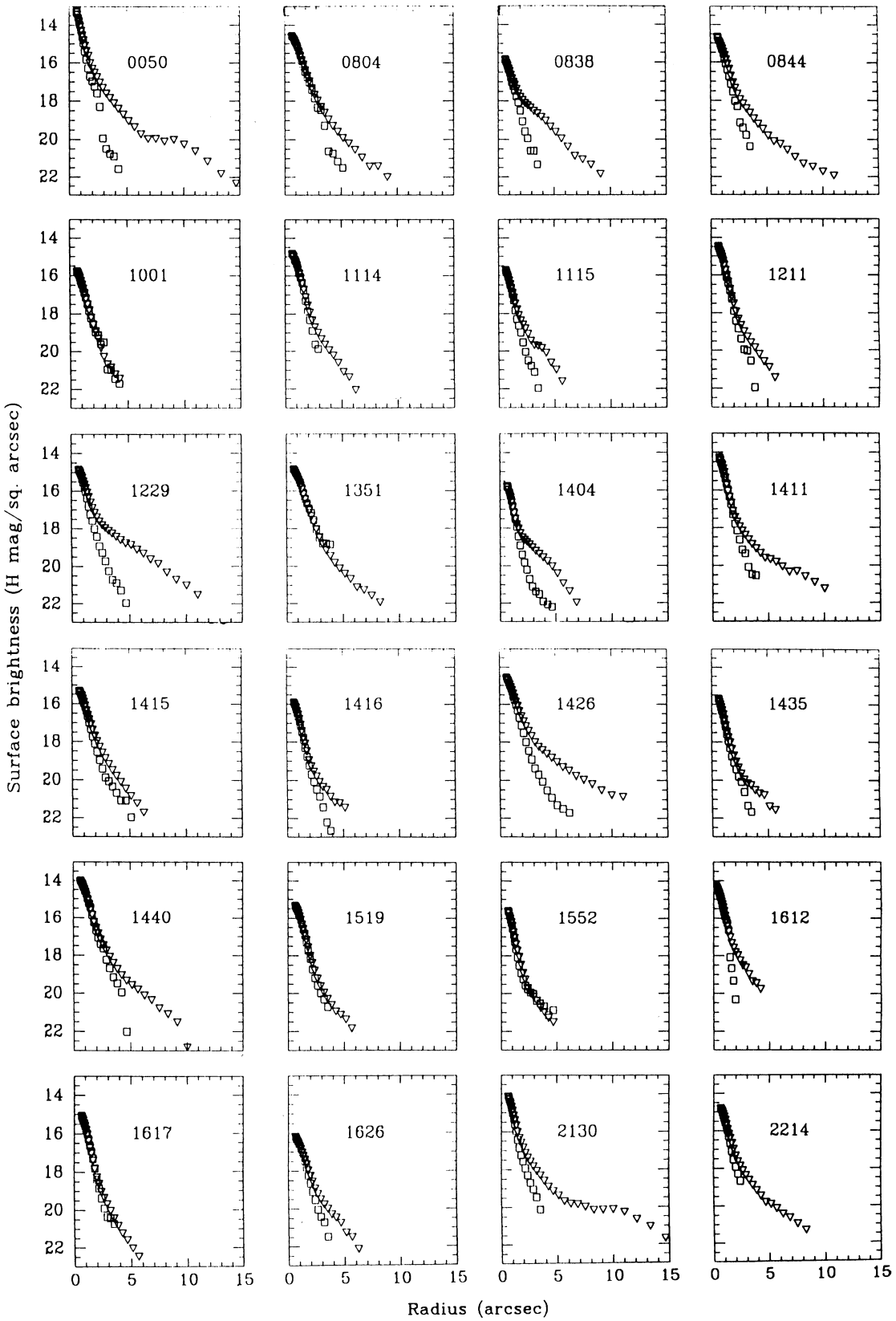

FIG. 2.—Radial profiles of QSOs (*triangles*) and normalized PSF stars (*squares*) plotted to S/N ≈ 1. Pixel scale is 0.″6 (0.″23 for PG 1612+261). PG 1001+054 and PG 1552+085 are unresolved.

TABLE 3

DISK FITS TO PROFILES

PG #	f[a]	s_0[b]	r_0[c]	H_{gal}[d]	H_{tot}[e]	H_{nuc}[f]	$\frac{L_{gal}(H)}{L_{tot}(H)}$ [g]
0050+124	0.85	15.0	1.33	12.42	11.37	11.88	0.378
0804+761	0.80	15.8	1.03	13.72	12.28	12.61	0.265
0838+770	0.70	17.0	2.05	13.40	13.38	17.71	0.981
0844+349	0.80	16.2	1.54	13.27	12.61	13.45	0.542
1001+054	0.80	≥16.1	0.56	≥15.36	13.95	≤14.30	≤0.273
1114+445	0.80	16.0	1.02	13.92	13.08	13.75	0.461
1115+407	0.75	16.9	1.23	14.47	13.73	14.49	0.506
1211+143	0.80	15.9	0.91	14.09	12.79	13.18	0.300
1229+204	0.85	16.9	2.70	12.70	12.47	14.23	0.804
1351+640	0.60	14.8	0.68	13.61	12.70	13.31	0.430
1404+226	0.75	17.7	2.09	14.09	13.80	15.36	0.762
1411+442	0.90	17.5	2.66	13.41	12.44	13.01	0.408
1415+451	0.85	16.6	1.16	14.27	13.22	13.73	0.377
1416−129	0.85	17.0	0.84	15.35	14.08	14.49	0.312
1426+015	0.90	16.5	2.15	12.81	12.15	13.00	0.544
1435−067	0.85	17.3	1.04	15.19	13.91	14.31	0.307
1440+356	0.85	16.6	1.82	13.34	11.90	12.24	0.267
1519+226	0.90	16.9	0.99	14.95	13.41	13.71	0.241
1552+085	0.85	≥16.1	0.59	≥15.29	13.93	≤14.29	≤0.284
1612+261[h]	0.45	14.5	0.61	13.58	13.27	14.80	0.754
1617+175	0.80	15.6	0.62	14.69	13.39	13.78	0.301
1626+554	0.85	17.9	1.70	14.74	13.89	14.55	0.456
2130+099	0.90	16.3	1.84	12.96	12.04	12.64	0.426
2214+139	0.90	16.6	1.73	13.38	12.66	13.45	0.516

[a] Fraction of normalized PSF subtracted.
[b] Central surface brightness of fitted galaxy (H_{mag} arcsec^{-2}).
[c] Disk scale length of fitted galaxy (arcsec).
[d] Total H magnitude of fitted galaxy.
[e] H magnitude of system (galaxy plus quasar nucleus).
[f] H magnitude of fitted PSF (i.e., quasar nucleus).
[g] Fraction of total H, band emission contributed by the host galaxy.
[h] Fine pixel data; flux calibration based on Neugebauer et al. (1987) photometry.

best fit. The derived galaxy flux was in general approximately twice the flux from the disk fit. In most cases, the disk fits were clearly very good, whereas the de Vaucouleurs fits were unacceptable in the outer parts of the profile. In several cases, disk and $r^{1/4}$ fits worked equally well. In three cases, however, the disk fits were poor where the de Vaucouleurs fits were much better. For the purposes of comparison with the rest of the sample, we have used the disk fits for these three objects. However, we will discuss these cases further below.

4. RESULTS

We have detected the quasar host galaxy in at least 22 out of the 24 cases. We estimate the errors in our total magnitudes to be about 0.1 mag, which is smaller than the uncertainty from the disk fits to the galaxies. Thus, based on the tests described above, we estimate that the galaxy H magnitudes are accurate to about 0.30 mag.

We have checked our photometry against the H photometry in Neugebauer et al. (1987) by adding up the light in a 5″ diameter aperture. Our magnitudes agree well with theirs, ours being on average 0.17 mag dimmer with 1 σ scatter about that average of 0.25 mag. The agreement is well within limits expected from the combined uncertainties and possible quasar variability except in the case of PG 1211+143 which we measure to be 0.7 mag dimmer than their value. We have used the Neugebauer et al. H fluxes to calibrate our data for PG 1612+261, because we did not observe a standard star with the fine pixel scale.

We have calculated absolute H magnitudes and sizes for the host galaxies assuming $H_0 = 80$ km s^{-1} Mpc^{-1} and $q_0 = 0$, and applying a small k-correction of $H(z) - H(0) = -0.02$ to -0.04 mag that is appropriate for the range of redshifts in our sample. The results are listed in Table 4, and we plot galaxy vs. total absolute magnitude in Figure 3. We estimated $M_H = -23.9$ for an L^* galaxy in a Schechter function description of the local field galaxy luminosity function, using an L^* magnitude of $M_V = -21.0$ (from, e.g., data of Efstathiou, Ellis, & Peterson 1988) and normal galaxy colors of $V-H = 2.9$. This color is appropriate for all but the latest type galaxies (Griersmith, Hyland, & Jones 1982; Aaronson 1977). By inspection of the Griersmith et al. data, we estimate the scatter in the $V-H$ color to be less than 0.2 mag (note, however, that these colors may be inappropriate for the outer disk regions). For the quasar host galaxies, $\langle M_H \rangle = -23.9 \pm 0.6$, where the quoted error is the 1 σ scatter around the mean. (In computing this value, we have set M_H for the two undetected galaxies equal to the upper limits on their luminosities.) Therefore, a typical low-luminosity quasar lies within an L^* galaxy as measured at H. Since the H luminosity traces the stellar mass, it appears that the host galaxies are of typical mass for field spirals.

The average disk scale length and central surface brightness are $\langle r_0 \rangle \approx 2.5$ kpc and 16.6 H mag arcsec^{-2} (but see caveats in § 5.1 below; surface brightness includes a small correction for galaxy inclination). The corresponding central surface brightness in V, 19.5 V mag arcsec^{-2}, is on the bright end of the

TABLE 4

ABSOLUTE MAGNITUDES[a]

PG #	M_H(gal)[b]	M_H(tot)[c]	s_0[d]	r_0[e]
0050+124	−24.4	−25.4	15.3	1.47
0804+761	−24.1	−25.6	15.9	1.87
0838+770	−25.0	−25.1	17.6	4.89
0844+349	−23.6	−24.3	16.5	1.80
1001+054	≥ −23.5	−25.0	≥16.2	1.64
1114+445	−24.7	−25.6	16.0	2.67
1115+407	−24.3	−25.1	17.1	3.45
1211+143	−23.4	−24.7	15.9	1.41
1229+204	−24.2	−24.4	17.4	3.15
1351+640	−23.9	−24.9	14.8	1.08
1404+226	−23.7	−24.0	18.3	3.73
1411+442	−24.2	−25.2	18.1	4.32
1415+451	−23.8	−24.9	16.6	2.40
1416−129	−23.0	−24.3	17.1	1.97
1426+015	−24.7	−25.4	16.8	3.36
1435−067	−23.2	−24.5	17.5	2.44
1440+356	−23.9	−25.4	16.7	2.55
1519+226	−23.6	−25.2	17.0	2.47
1552+085	≥ −22.9	−24.3	≥16.3	1.27
1612+261	−24.8	−24.9	14.8	1.45
1617+175	−23.4	−24.8	15.7	1.28
1626+554	−23.7	−24.6	17.9	4.12
2130+099	−23.8	−24.8	17.1	2.04
2214+139	−23.6	−24.3	16.6	2.11

[a] $H_0 = 80$ km s^{-1} Mpc^{-1} and $q_0 = 0$.
[b] Absolute magnitude of fitted galaxy; includes k-correction.
[c] Total magnitude of system.
[d] Central surface brightness of fitted galaxy (H mag arcsec^{-2}); includes inclination correction.
[e] Disk scale length of fitted galaxy (kpc).

distribution measured by Kent (1985), whereas the disk scale length we have measured is typical of his sample. Those results reinforce the conclusion that the host galaxies are typical spirals.

We have also used the normal galaxy colors described above to determine our surface brightness detection limit, $B \approx 25$ mag arcsec^{-2}. Though CCD studies can go several magnitudes deeper, our limit is sensitive enough for comparison with other galaxy studies, which often quote results to a surface brightness $B = 25$ mag arcsec^{-2}. Based on the data given in Smith et al. (1986), we find that the average nuclear-to-galaxy luminosity ratio at visible wavelengths is nearly 5, while our H-band results give a value less than 2; thus, the behavior of the SEDs favors the use of IR imaging to study host galaxies.

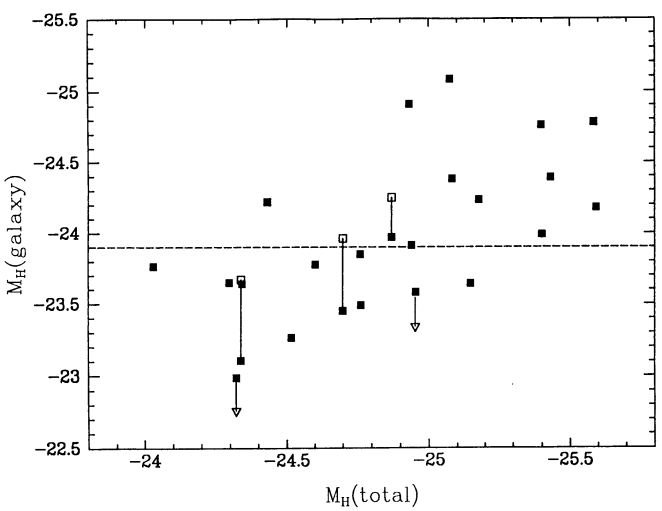

FIG. 3.—Plot of galaxy vs. total magnitude in the H band ($H_0 = 80$ km s^{-1} Mpc^{-1}). The dotted line shows the magnitude of an L^* galaxy. Filled squares represent disk fits; open squares represent the preferred $r^{1/4}$ fits for three galaxies discussed in the text.

5. DISCUSSION

5.1. *Disk Fits*

The exponential disk models should be considered only a first approximation to the galaxy luminosity profiles. With high-resolution optical images, many quasars are seen to be morphologically disturbed by tidal interactions (e.g., Hutchings & Neff 1992), so we might not expect an exponential disk or $r^{1/4}$ model to be appropriate. Where the galaxy is faint, very deep images are required to distinguish between these models, even if the galaxy is undisturbed.

There are, however, reasons to expect that disk models are an appropriate approximation. First, adopting the radio-quiet/radio-loud quasar cutoff as defined by Woltjer (1990), $P_{5\ \mathrm{GHz}} = 10^{24.7}$ W Hz^{-1}, we find that all of the objects in our sample are radio-quiet and hence possibly associated with disk galaxies. The radio power of each quasar, taken from Kellerman et al. (1989), is listed in Table 1. Second, we might expect a distributed galaxy to look less peculiar in near-IR, mass-tracing light than in optical light. Third, the redshift of these objects is so low that the $\sim 1''$ resolution of our data should be adequate. Finally, the disk models do fit most of the profiles well, whereas $r^{1/4}$ models were often unacceptable.

Thus, we caution that it may be dangerous to interpret the scale lengths and central surface brightness as spiral galaxy parameters. However, we believe that the fits accurately account for the galaxy light, so that the end products of the fits, namely the galaxy magnitudes, are robust.

Interestingly, we find that two of the three galaxies in which a de Vaucouleurs profile was preferred over a disk profile are associated with relatively strong radio emitting quasars, PG 1351+640, and PG 1461−129. Even with the $r^{1/4}$ fits, the three galaxies have luminosities near those of L^* galaxies. The average M_H for the galaxies assuming $r^{1/4}$ fits is $\langle M_H \rangle = -23.9$, the same as that for the whole sample. If these galaxies are included in the sample average at their $r^{1/4}$ values, we still obtain $\langle M_H \rangle = -23.9$, i.e., approximately the L^* value.

5.2. *Galaxy Ellipticities*

From the elliptical isophote fits to the quasar images, we are able to determine the ellipticity $\epsilon = 1 - b/a$ from the axis ratio b/a. We find on average $\epsilon = 0.2$ with all galaxies having $\epsilon < 0.5$. This lack of flattened galaxies was also found for the sample of quasars imaged at K by Dunlop et al. (1993), who note that there "appears to be a selection bias against finding active nuclei in an edge-on disc" galaxy. Given the minimal overlap of their sample with ours, our result provides an independent confirmation of the effect. Hutchings et al. (1989) had also noted this tendency from imaging in the visible. Presumably, it indicates that quasars in edge-on galaxies are too reddened to be included in visible light surveys such as the PG survey. Assuming a simple geometry where there is a sharp cutoff in quasar visibility at $\epsilon = 0.5$ and no effect for $\epsilon < 0.5$, only 50% of the sky is visible to the quasar in the usual optical search techniques. Therefore, typical searches must underesti-

mate the space density of quasars like the low-luminosity ones we have studied by a factor of ~ 2.

It is interesting to speculate where the obscuration of the quasar occurs. An ellipticity $\epsilon = 0.5$ corresponds to an inclination angle of 60°. Given their small scale heights, disks do not extend close enough to the galaxy nucleus to obscure it at this inclination. Thus the obscuration is probably close to the active nucleus.

5.3. *Comparison to CCD Studies*

We now compare our results to previously published information about QSO host galaxies. In the following discussion, we have adjusted all results to $H_0 = 80$ km s^{-1} Mpc^{-1}. We refer to the summary by VW, who have assembled data for approximately 40 radio-quiet quasars and Seyferts from their own sample and the samples of Malkan (1984), Malkan, Margon, & Chanan (1984), Smith et al. (1986), & Gehren et al. (1984). These data provide a good comparison to our sample because the objects have low redshifts and because the galaxy magnitudes are based on disk fits to the profiles. The 12 QSOs with the same luminosity as the QSOs in our sample have mean redshift $\langle z \rangle = 0.167$ and mean galaxy magnitude $\langle M_V \rangle \approx -21.5$, with a scatter of 0.8 mag. By comparison, in our sample the average magnitude would correspond to $\langle M_V \rangle \approx -21.0$ with normal galaxy $V-H$ colors. Thus, if the two samples represent the same population of objects, we find that the $V-H$ colors we assumed are inappropriate and that the host galaxies are about a half a magnitude bluer in $V-H$ than normal early-type galaxies.

The sample of radio-quiet QSOs observed by Hutchings et al. (1989) unfortunately does not provide as good a comparison for our sample; only eight of those objects have a B luminosity in the range represented in our sample, and their average redshift is nearly 0.3. The average galaxy magnitude of these objects is $\langle M_V \rangle \approx -21$ with a large scatter of 1.5 mag (derived from B magnitudes, including an uncertain k-correction). The large scatter and different sample properties make this result difficult to interpret.

In several cases, magnitudes for galaxies in our sample have been measured using CCDs. As reported in VW, the QSO PG 2130+099 = II Zw 136 has been imaged by three different groups (Smith et al. 1986; Gehren et al. 1984; Malkan 1984) with an average galaxy magnitude measured to be $M_V = -21.4$. Using our value $M_H = -23.8$ for the galaxy we compute $V-H = 2.4$, which is half a magnitude bluer than normal early-type galaxies. Similarly, using published visible magnitudes for the hosts of PG 0050+124, PG 1440+356, PG 2214+139, and PG 1626+554 (Smith et al. 1986; Malkan 1984; Hutchings et al. 1988), we find that these galaxies are about a magnitude bluer in $V-H$ than normal early-type galaxies. Two quasars, PG 0844+349 and PG 1612+261, are found to have normal or slightly red hosts (Hutchings & Crampton 1990; Hutchings et al. 1988).

These colors suggest that many, but not all, of the galaxies have undergone strong star formation, making them bluer than normal galaxies. Any correlations seen in CCD studies between galaxy and nuclear luminosity apply only to the blue stellar component; CCDs probably trace out a young, blue, stellar population that is somehow associated with the activity in the nucleus. Indeed, optical spectroscopy of the host galaxies of some of our objects shows evidence for a young stellar component (Hickson & Hutchings 1987; Hutchings & Crampton 1990).

5.4. *Galaxy Mergers*

In normal galaxies, the near-IR output arises from red giant stars that have evolved from the stellar population that dominates the galaxy mass. Therefore, the luminosity at H is a measure of the stellar mass of the galaxy. In galaxies which have undergone large starbursts, massive red giants and red supergiants can increase the H luminosity temporarily. Hence, for the quasar host galaxies, which have evidence for some degree of active star formation, we take the H luminosities to provide an upper limit to the stellar masses when compared with normal galaxies.

It is therefore remarkable that the host galaxies in our sample typically have the H luminosities of L^* galaxies. Out of the 24 galaxies, 16, or $\approx 70\%$, have M_H fainter than $M_{L*} - 0.3$ (where 0.3 mag is the size of the galaxy magnitude uncertainties). Even if our photometry is subject to a 0.17 mag zero-point shift as might be indicated by the Neugebauer et al. (1987) photometry, 15 galaxies still satisfy this criterion. This result appears *not* to be compatible with the hypothesis that these quasars originate from the activity triggered by the merger of two large, gas-rich spiral galaxies.

To make a more detailed comparison with merger/starburst expectations, we have used the starburst program described by Rieke et al. (1993). We computed a model of a short-duration starburst using the initial mass function of Scalo (1986) and let it evolve for 10^8 yr. We then combined it with normal galaxy colors to reproduce the observed $V-H \approx 2.4$ for the quasar hosts. The starburst has $V-H \approx 1.65$ at the age, and we assumed $V-H = 2.9$ for the underlying galaxy.

Using these colors, we divided the average $\langle M_H \rangle = -24$ for our sample into underlying and starburst components. We determined the average H luminosity for the underlying galaxies to be $\langle M_H \rangle = -23.65$. Therefore, the possibility that the hosts represent mergers of two "normal" L^* galaxies is even less likely. For the starburst component, $\langle M_H \rangle = -22.6$, which corresponds to a bolometric luminosity at the peak of the starburst of $L_{\rm bol} = 9 \times 10^{11}\ L_\odot$. $L_{\rm bol}$ would exceed $4 \times 10^{11}\ L_\odot$ for 10^7 yr in these models. If the starburst IMF were biased toward massive stars, these luminosities would increase.

If the age of the starburst is increased beyond 10^8 yr, its stellar population becomes redder. To match the total colors, the host galaxy luminosity must then be significantly less than that of a single L^* galaxy. If the age of the starburst is 5×10^7 yr, the $V-H$ colors can be reproduced with the average of $\langle M_H \rangle = -23.75$ for the underlying galaxy. Making the starburst younger than 5×10^7 yr results in decreasing the permitted host H luminosity (because the starburst emission is dominated by extremely luminous red stars), unless it is only a few million years old. Such young starbursts are not plausible for the average properties of our sample. We conclude that the galaxy properties are consistent with the host having been the site of a very luminous starburst about 10^8 yr ago. However, this event must have occurred within a single $\sim L^*$ galaxy, not through the merger of two such galaxies. One possibility is that star formation and quasar activity was triggered by the interaction of an L^* galaxy with a substantially less massive companion. Such interactions have been described by Hutchings (1987), who found that companions to quasars in his sample are always fainter and smaller than the host galaxies (note, however, that those are radio-loud quasars). Alternatively, the relatively blue $V-H$ colors may result from an ongoing episode of star formation rather than a burst.

5.5. *Comparison to Other Near-IR Studies*

Combining our H data with the Dunlop et al. (1993) K data for the three objects common to both studies gives puzzling results. They have given K magnitudes for the galaxies surrounding PG 1211+143, PG 1440+356, and PG 2130+099. The technique they use to obtain the galaxy magnitude is to subtract the PSF so that the flux in the central pixel goes to zero. To compensate for this oversubtraction, they suggest a 0.75 mag adjustment to the galaxy magnitudes. The resulting magnitudes give $H-K \approx 1$ mag, which is surprisingly higher than the k-corrected value for "normal" galaxies, ≈ 0.45.

Zitelli et al. (1993) have recently presented K-band radial profiles for a sample of Seyfert 1 galaxies, including four of the galaxies in our sample: PG 0050+124 (I Zw I), PG 1440+356 (Mrk 478), PG 2130+099 (II Zw 136), and PG 2214+139 (Mrk 204). The K radial profiles agree fairly well with our H profiles outside the region where the nucleus contributes. However, the galaxy colors implied by these profiles are $H-K \approx 1$ mag. These authors also obtained H-band photometry in a 5″ diameter beam for the latter two of these objects; their photometry agrees with ours to within 0.2 mag. The photometric agreement makes the peculiar colors difficult to interpret.

We feel that the very red colors may result from the different ways the data were obtained and reduced. To test this hypothesis, we obtained K images of four quasars in our sample. The data were obtained with the same instrument setup and telescope as the H data and were reduced and processed using the same techniques. The resulting $H-K$ colors are consistent with the expected values; they are not anomalously red.

6. SUMMARY

We have taken H-band images for a complete sample of 24 low-luminosity QSOs with redshift $z \lesssim 0.15$. We have detected the host galaxy for at least 22 of these objects. We find the following.

1. Most of the galaxies have surface brightness profiles that follow an exponential disk law;
2. On average, the galaxy contributes about 40% of the total light in the H band;
3. The average H magnitude, and hence mass, is that of an L^* galaxy;
4. The galaxies are bluer than normal early-type galaxies by about 0.5 mag in $V-H$;
5. The blue colors are consistent either with the galaxies having undergone very luminous starbursts about 10^8 yr ago, or with an ongoing episode of star formation in the galaxies;
6. Most of these sources cannot arise from mergers of two normal L^* spiral galaxies;
7. About half of the low-luminosity quasars are hidden by obscuration that is probably close to the active nucleus; the space density of these sources is probably underestimated by a factor of ~ 2.

We are grateful to the referee, J. B. Hutchings, for helpful comments. We also thank Todd Boroson and Jill Bechtold for useful discussions; Marcia Rieke and Brian McLeod for providing some to the image reduction software; and Doug Williams and Bill Latter for observing some of our objects. The data reduction and analysis described here were carried out using the Image Reduction and Analysis Facility—thanks to Ivo Busko for fixing up the IRAF ellipse fitting task. This material is based upon work supported under a National Science Foundation Graduate Fellowship and under NSF grant AST-9116442.

REFERENCES

Aaronson, M. 1977, Ph.D. thesis, Harvard Univ.
Boroson, T., Persson, S., & Oke, J. B. 1985, ApJ, 293, 120
Dunlop, J. S., Taylor, G. L. Hughes, D. H., & Robson, E. I. 1993, MNRAS, in press
Efstathiou, G., Ellis, R. S., & Peterson, B. A. 1988, MNRAS, 232, 431
Elias, J. H., Frogel, J. A., Matthews, K., & Neugebauer, G. 1982, AJ, 87, 1029
Gehren, T., Fried, J., Wehinger, P. A., & Wyckoff, S. 1984, ApJ, 278, 11
Griersmith, D., Hyland, A. R., & Jones, T. J. 1982, AJ, 87, 1106
Hickson, P., & Hutchings, J. B. 1987, ApJ, 312, 518
Hutchings, J. B. 1987, ApJ, 320, 122
Hutchings, J. B., & Crampton, D. 1990, AJ, 99, 37
Hutchings, J. B., Crampton, D., & Campbell, B. 1984, ApJ, 280, 41
Hutchings, J. B., et al. 1984, ApJS, 55, 319
Hutchings, J. B., Janson, T., & Neff, S. G. 1989, ApJ, 342, 660
Hutchings, J. B., Johnson, I., & Pyke, R. 1988, ApJ, 66, 361
Hutchings, J. B., & Neff, S. G. 1992, AJ, 104, 1
Kellerman, K. I., Sramek, R., Schmidt, M., Shaffer, D. B., & Green, R. 1989, AJ, 98, 1195
Kent, S. M. 1985, ApJS, 59, 115
Kotilainen, J. K., Ward, M. J., Boisson, C., DePoy, D. L., Bryant, L. R., & Smith, M. G. 1992, MNRAS, 256, 125
Malkan, M. A. 1984, ApJ, 287, 555
Malkan, M. A., Margon, B., & Chanan, G. A. 1984, ApJ, 280, 66
Miller, P., Rawlings, S., & Saunders, R. 1993, MNRAS, 263, 425
Neugebauer, G., Green, R. F., Matthews, K., Schmidt, M., Soifer, B. T., & Bennett, J. 1987, ApJS, 63, 615
Rieke, G. H., Loken, K., Rieke, M. J., & Tamblyn, P. 1993, ApJ, 412, 90
Sanders, D. B., Phinney, E. S., Neugebauer, G., Soifer, B. T., & Matthews, K. 1989, ApJ, 347, 29
Scalo, J. M. 1986, Fund. Cosmic Phys., 11, 1
Schmidt, M., & Green, R. F. 1983, ApJ, 269, 352
Smith, E. P., Heckman, T. M., Bothun, G. D., Romanishin, W., & Balick, B. 1986, ApJ, 306, 64
Véron-Cetty, M.-P., & Véron, P. 1984, ESO Sci. Rep. 1
Véron-Cetty, M. P., & Woltjer, L. 1990, A&A, 236, 69 (VW)
Woltjer, L. 1990, in Active Galactic Nuclei, ed. T. J.-L. Couorvoisier & M. Mayor (Heidelberg: Springer), 1
Zitelli, V., Granato, G. L., Mandolesi, N., Wade, R., & Danese, L. 1993, ApJS, 84, 185